

Brightening of the exciton ground state in carbon nanotubes in the strong light-matter coupling regime

V. Shahnazaryan,^{†,‡} V. A. Saroka,^{¶,§} I. A. Shelykh,^{†,||} and M. E. Portnoi*,[¶]

[†]*ITMO University, St. Petersburg 197101, Russia*

[‡]*Russian-Armenian (Slavonic) University, Yerevan 0051, Armenia*

[¶]*School of Physics, University of Exeter, Stocker Road, Exeter EX4 4QL, United Kingdom*

[§]*Institute for Nuclear Problems, Belarusian State University, Bobruiskaya 11, 220030*

Minsk, Belarus

^{||}*Science Institute, University of Iceland IS-107, Reykjavik, Iceland*

E-mail: M.E.Portnoi@exeter.ac.uk

Abstract

We propose a scheme to maintain a robust radiative ground state in semiconductor single-walled carbon nanotubes. For that purpose, we employ a microcavity operating in the regime of strong coupling between the confined electromagnetic mode of the cavity and the excitonic resonance in an ensemble of carbon nanotubes. A high value of the interband dipole matrix element in nanotubes makes the light-matter interaction extremely efficient and enables the achievement of the ultra-strong coupling regime. Radiative excitonic states become dressed by cavity photons and form polariton states which experience a huge vacuum Rabi splitting. The energy of the lower polariton moves downwards and can go beneath the energy of the dark exciton, and thus the ground state of the system becomes radiative. This leads to the radical enhancement

of luminescence and opens new perspectives for potential optoelectronic applications of carbon-nanotube-based structures.

Single-walled carbon nanotubes (SWCNTs), discovered more than two decades ago,¹ possess a set of remarkable electronic and optical properties.² Despite this fact, their practical applications are so far very limited.^{3,4} This is partially connected to the difficulties of selectively synthesising SWCNTs with a predefined chirality. However, recent technological progress has opened such a possibility for (6,6) SWCNTs⁵ (see Ref.⁶ for nanotube classification). At the same time, the post synthesis sorting methods, such as multi-column gel chromatography, and SWCNT alignment techniques have improved significantly.⁷⁻⁹ Nevertheless, a number of more fundamental problems which hinder the efficient use of SWCNTs in optoelectronics still persist.

One such problem is a drastic suppression of photoluminescence from nanotubes, even at room temperature.¹⁰ The reason is the presence of a non-radiative dark exciton state, which has a significantly lower energy than the radiative bright excitonic states.¹¹⁻¹³ This leads to the fact that for the bright excitons the relaxation towards the dark ground state, and then its non-radiative decay, dominates over the radiative relaxation channel.^{14,15} Possible routes to enhance photoluminescence efficiency include breaking time-reversal symmetry by applying an external magnetic field,¹⁶⁻¹⁸ chemical functionalization¹⁹ or by exploiting high-power pulsed-laser irradiation at room temperature.²⁰ However, due to the small tube diameter, magnetic brightening requires magnetic fields of about 5-50 T^{18,21} or pulsed fields of up to 190 T.²² Theoretically proposed brightening by chemical functionalization relies on the precise control of binding and the orientation of covalent functionalization of semiconducting SWCNTs and can hardly be achieved with the current state of technology. Irradiation brightening requires strong laser fields which leads to irreversible damage to the tubes.

In this paper we propose an alternative approach to the problem of ground state brightening, based on the achievement of the strong coupling regime between bright excitons in an ensemble of SWCNTs and the confined electromagnetic mode of a microcavity. The

technological task of embedding nanotubes inside high quality microcavities is currently reachable²³⁻²⁵ which makes our proposal experimentally feasible.

The strong light-matter coupling regime is achieved when the characteristic coupling energy of the interaction between material excitations and light exceeds energy broadenings appearing due to the losses in the system. In this situation, hybrid light-matter particles, known as polaritons, are formed in the system. The conventional polaritonic setup implies a planar microcavity with semiconductor²⁶ or organic quantum wells.²⁷⁻³⁰ The use of organic materials allows one to reach higher Rabi splittings because of the intrinsically large binding energies and oscillator strengths of the excitons.

It was recently experimentally demonstrated that the regime of strong coupling can be realized for ensembles of carbon nanotubes.³¹⁻³³ In the current paper we consider the following problem: can the achievement of strong coupling regime lead to a fundamental change to the nature of the ground state of the system? Such a change is indeed possible: due to the coupling with cavity mode, the bright excitonic state is split into lower and upper polaritons separated by the value of Rabi splitting Ω_R . If half of the latter quantity exceeds the value δ of the splitting between the dark and bright excitons, $\Omega_R > \delta$, as is shown at Fig. 1(c), the lower polariton state sinks below the dark exciton and the ground state thus becomes radiative. The characteristic splitting between dark and bright excitons is usually several tens of meV, thus brightening of the ground state requires the achievement of Ω_R in the range 50-100 meV or above. We demonstrate that this criterion can be met in experimentally realizable configurations, similar to those presented in Refs.³¹⁻³³

Exciton states. Estimating the value of the Rabi splitting for nanotube-based systems requires the knowledge of parameters characterizing excitons in a single nanotube, such as the exciton binding energy and oscillator strength. For their estimation, different theoretical approaches, with varying degree of complexity, were proposed: numerical results were obtained in the framework of $\mathbf{k} \cdot \mathbf{p}$ effective mass models,^{17,34-38} first principles calculations,^{11,39,40} solutions of the Bethe-Salpeter equation in the tight-binding approxima-

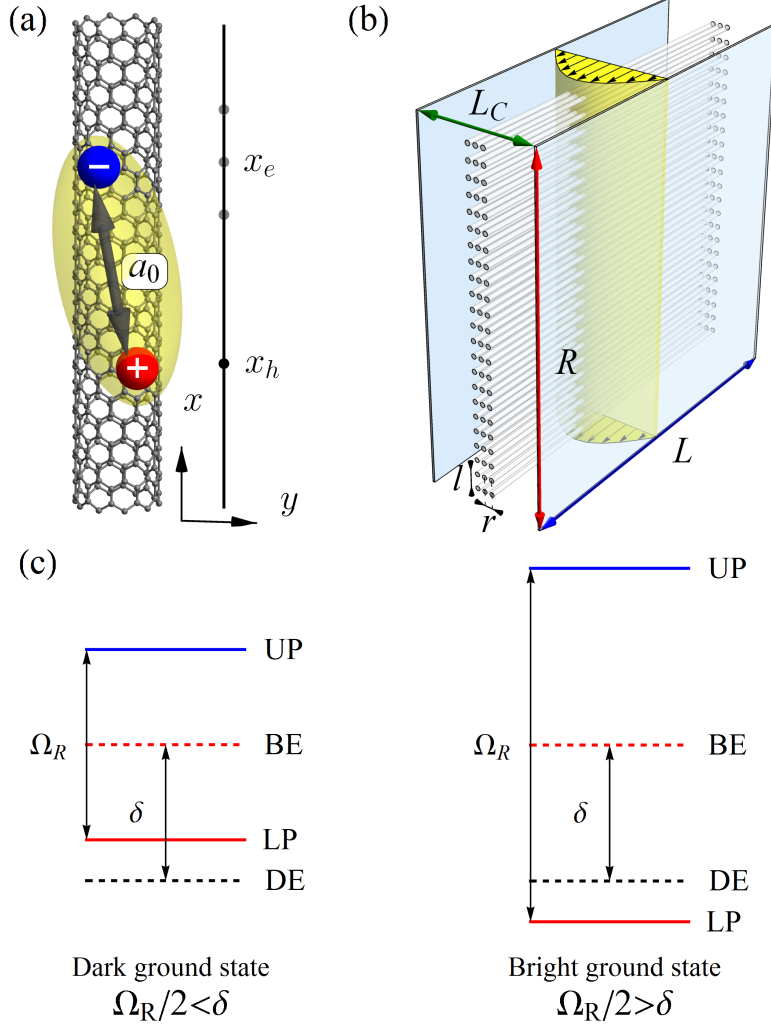


Figure 1: (a) A sketch of a semiconductor carbon nanotube containing an exciton (bound electron-hole pair) and its 1D mathematical model. The characteristic size of the pair is the excitonic Bohr radius a_0 . (b) The geometry of the structure considered in the present paper: a planar microcavity with an array of aligned carbon nanotubes embedded in a position such that the electric field of the confined cavity mode (shown in yellow) reaches its maximum. Strong coupling between bright excitons and confined photons leads to the formation of hybrid polariton modes in the system. (c) The mechanism of brightening. Strong light-matter coupling leads to the hybridization of the bright exciton (BE) and photonic modes, resulting in the appearance of upper (UP) and lower (LP) polaritons separated by the value of the Rabi splitting Ω_R . If $\Omega_R/2 < \delta$, where δ is splitting between bright and dark excitons (DE), the ground state remains dark (left side of the panel). However, if $\Omega_R/2 > \delta$, the energy of the lower polariton sinks below the energy of the dark exciton and the ground state brightens.

tion,^{12,13,41} Pariser-Parr-Pople models⁴² and variational approaches.^{43,44} Besides, analytical solutions of two-particle problems have been found for some classes of model interaction potentials.^{45,46}

In the present work we use a combination of the effective-mass and envelope-function approaches along with the low-energy zone-folding tight-binding model. In this case the electron-hole interaction in the tube can be approximated by a shifted Coulomb potential^{47,48}

$$V(x) = -\frac{1}{4\pi\epsilon_0\epsilon_C} \frac{e^2}{(|x| + \gamma d)}, \quad (1)$$

where $x = x_e - x_h$ is the distance between electron, x_e , and hole, x_h , positions on the nanotube axis as shown in Fig. 1(a), d is the diameter of the nanotube, e is elementary charge, ϵ_0 is the electric constant and $\epsilon_C = 2$ is the static dielectric constant of the carbon nanotube.^{41,42} The Coulomb interaction (1) in general mixes all of the subbands, but for tubes with moderate diameters ($d < 2$ nm) the subbands extrema are well separated in energy and a two-band model can be used. When $d \ll a_0$, where a_0 is the characteristic size of an exciton, the problem becomes equivalent to the phenomenological analytical model of a 1D exciton developed by Loudon⁴⁷ and successfully applied to the description of excitons in semiconducting quantum wires⁴⁹⁻⁵¹ and semiconducting carbon nanotubes.⁴⁸ To determine the cutoff scaling parameter γ in Eq. (1) we analyzed numerical and experimental data on exciton binding energies from Refs.^{39,42-44} In Loudon's model, the binding energy of the exciton is related to the exciton quantum number α , which can be fractional due to a quantum defect, via⁴⁷

$$E_b = -\frac{\hbar^2}{2\mu a_0^2 \alpha^2}. \quad (2)$$

where $a_0 = 4\pi\epsilon_0\epsilon\hbar^2/(\mu e^2)$ is the excitonic Bohr radius and $\mu = m^*/2$ is the reduced mass of an electron-hole pair. The effective masses of an electron and a hole are equal, and within the tight-binding model can be estimated as $m^* = (2\hbar)/(3dv_F)$, with v_F being the Fermi velocity in graphene. Extracting α 's for known E_b 's from Eq. (2) and averaging them for

ground states of various SWCNTs ($\alpha_{av.} = 0.649$), one obtains (via Eq. (3.22) in Ref.⁴⁷) the cutoff scaling parameter $\gamma = 0.875$. It should be mentioned, that this value is essentially different from that in Ref.,⁴⁸ where γ was fixed to be 0.3 and the static dielectric constant was used as an adjusted parameter in Loudon’s model. We employ a slightly different approach to the problem, since we assume that the static dielectric constant in all experiments should be mainly defined by the carbon nanotube dielectric constant ε_C and as such cannot be tuned throughout the set of experimental data. Additionally, the value of the dielectric constant averaged over various experiments is problematic for physical interpretation. We use the estimated γ and α to calculate the excitonic wave function, which is expressed in terms of the Whittaker function of the second kind as⁴⁷

$$\psi_\alpha(x) = N_\alpha W_{\alpha,1/2}(2(|x| + \gamma d)/\alpha a_0) \quad (3)$$

with N_α being the normalization constant. It is easy to check that the ratio d/a_0 is universal for all diameters of the tubes and takes the value of $d/a_0 = 0.372$ for realistic parameters.

Table 1: Nanotube diameters d , exciton effective masses μ , bandgaps E_g , exciton binding energies E_b and coupling constants between the excitons and confined cavity mode g for SWCNTs of different chiralities. The values of g were calculated for the case of the resonance between photons and bright excitons for an inter-tube separation corresponding to 3 nm.

SWCNT	d (nm)	μ (m_0)	E_g (eV)	E_b (eV)	$g(0)$ (meV)
(7,0)	0.548	0.072	1.57	0.564	68.69
(6,2)	0.565	0.069	1.53	0.555	68.43
(8,0)	0.626	0.062	1.38	0.499	64.81
(6,4)	0.683	0.057	1.26	0.459	60.99
(9,1)	0.747	0.052	1.15	0.419	58.66
(6,5)	0.747	0.052	1.15	0.419	58.66
(8,3)	0.771	0.051	1.12	0.411	57.86
(10,0)	0.783	0.050	1.10	0.403	57.05
(7,5)	0.818	0.048	1.05	0.386	55.91
(11,0)	0.861	0.045	1.00	0.362	54.56
(7,6)	0.882	0.045	0.98	0.362	54.08
(9,4)	0.903	0.043	0.95	0.346	52.85
(13,0)	1.020	0.038	0.85	0.306	50.74
(14,0)	1.100	0.036	0.79	0.290	48.96

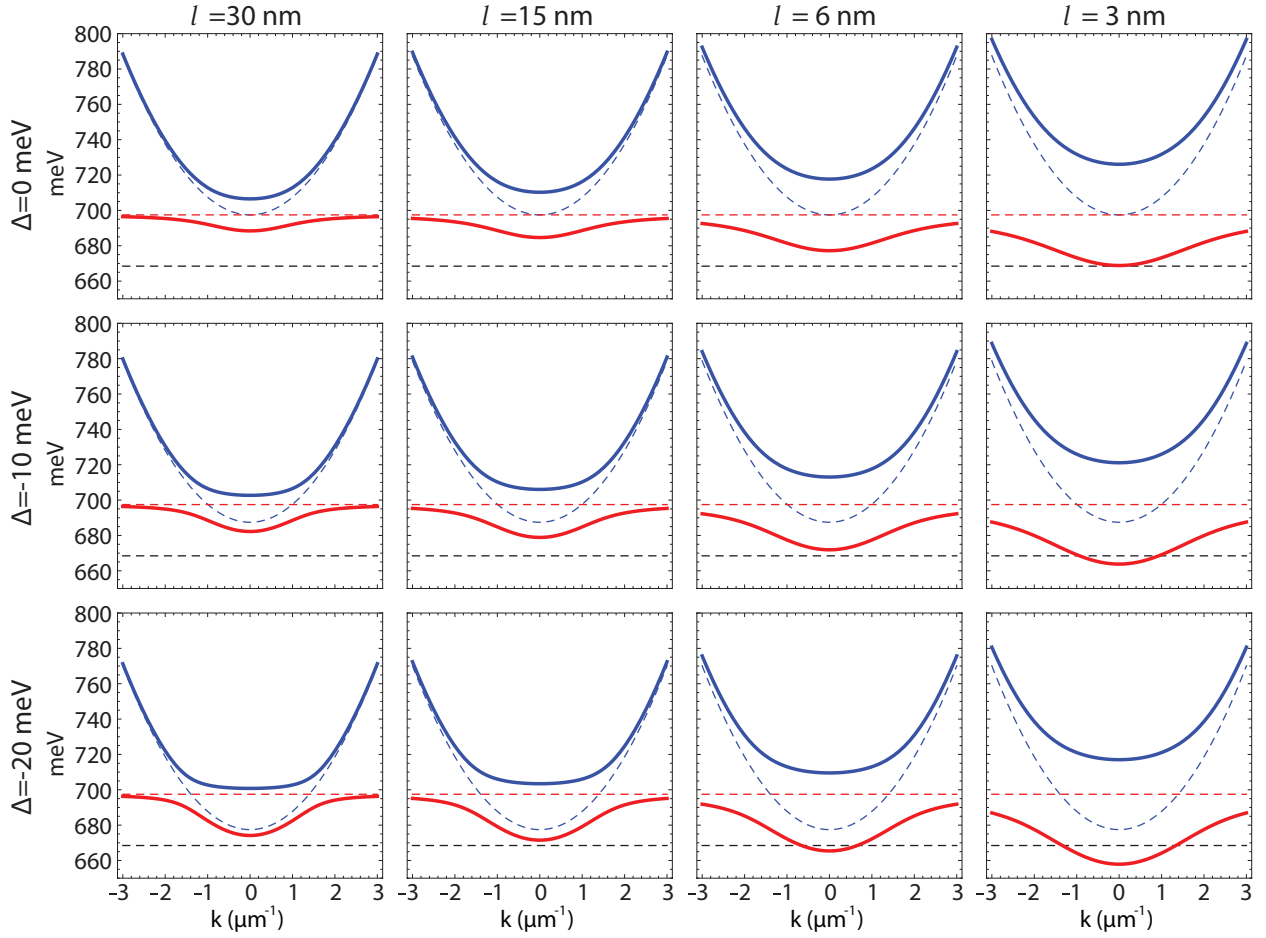


Figure 2: The dispersions of the polariton modes versus those of bare excitons and cavity photons for different detunings (from top to bottom) and nanotube separation distances (from left to right) for the case of a (10,0) SWCNT. The dashed lines correspond to the bare photon (blue), bright exciton (red) and dark exciton (black) modes, solid red and blue lines correspond to the upper and lower polaritons, respectively. One clearly sees that the decrease of the inter-tube separation results in the increase of the Rabi splitting. Consequently, the lower polariton mode moves down in energy and for certain separations can cross the dark exciton. In this situation the brightening of the ground state of the system takes place.

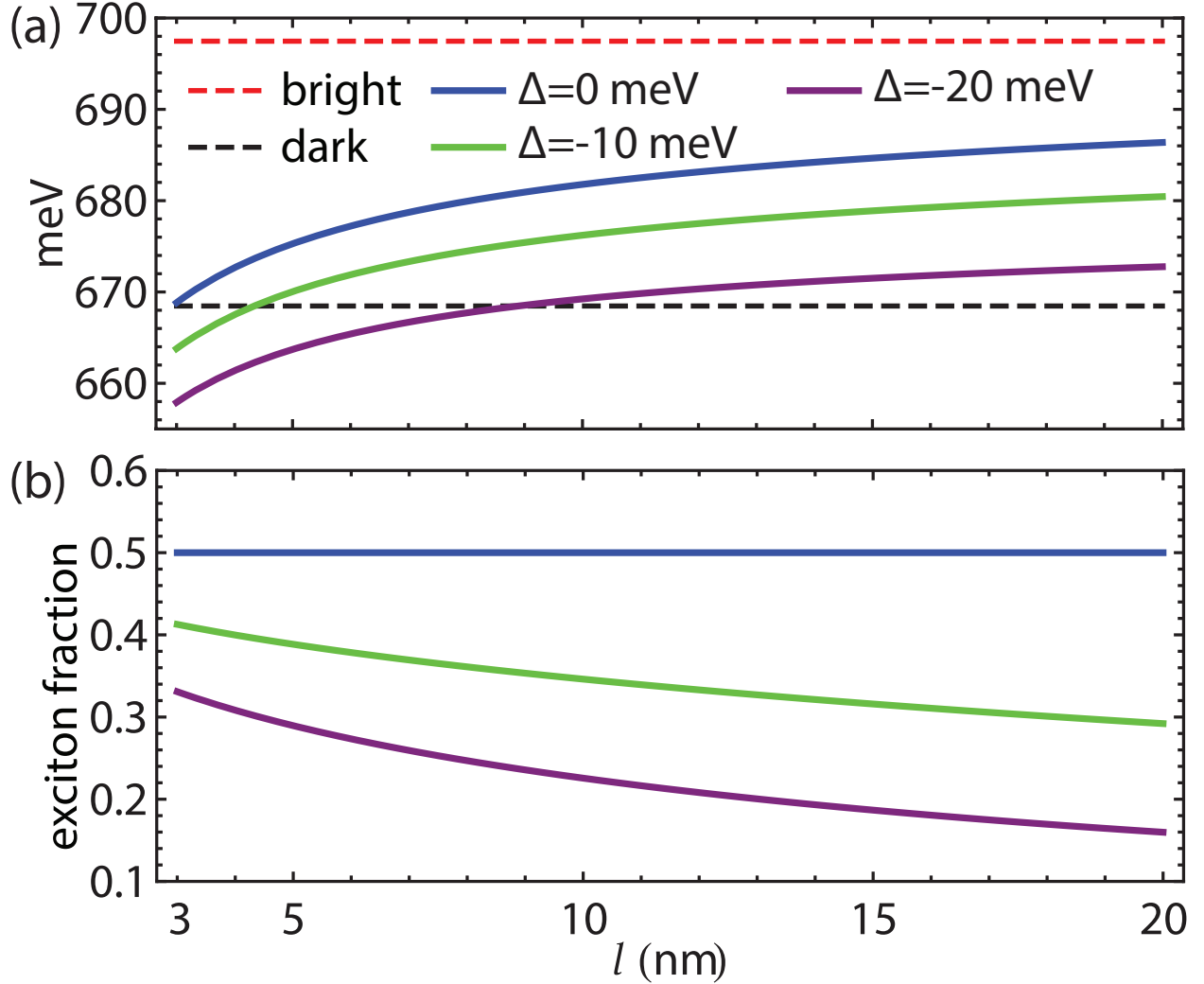


Figure 3: (a) The position of the bottom of the lower polariton branch as function of the inter-tube distance l , for the case of a (10,0) SWCNT, for different detunings versus dark exciton energy (dashed black line). For small values of l the lower polariton lies below the dark exciton and the ground state brightens. (b) Exciton fraction in the lower polariton mode as a function of the inter-tube distance l for the case of a (10,0) SWCNT for different detunings. Even for detunings as large as 20 meV this fraction remains substantial, which is a direct consequence of the large values of the Rabi splitting Ω_R .

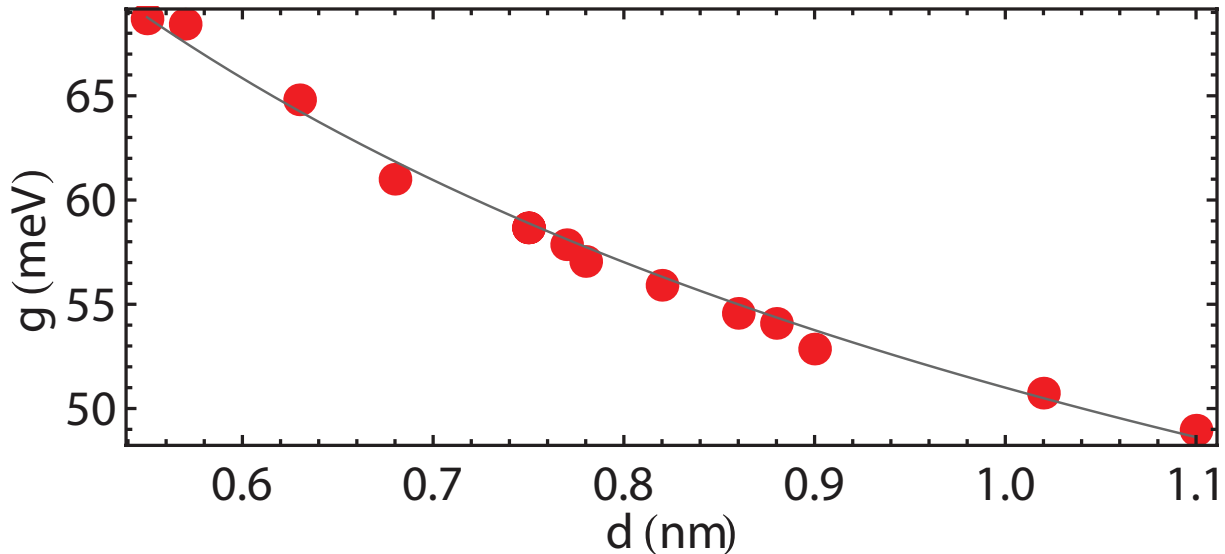


Figure 4: The dependence of the light-matter coupling constant on the nanotube diameter. The decrease of diameter leads to the increase of the light matter coupling. Red points correspond to our numerical data, the black curve is a numerical fit corresponding to a $d^{-1/2}$ scaling. The tube separation distance was chosen as $l = 3$ nm and the detuning $\Delta = 0$.

Polariton states. The structure under consideration consists of an array of SWCNTs embedded into a planar microcavity formed by a pair of distributed Bragg reflectors (DBRs) (see Fig. 1 (b)). The majority of the results presented in this paper are obtained for a zigzag structure with chirality (10,0). We note, however, that the developed approach is of a general character and can be applied for semiconducting nanotubes of an arbitrary configuration. Our analysis of the chirality dependence of the light-matter coupling constant will be presented later on.

The energy corresponding to photoexcitation of an exciton is defined as $E_X = E_g - E_b$ where E_g is the value of the bandgap and E_b is the exciton binding energy calculated within the model described above. In order to enhance the light-matter coupling regime, one needs the cavity mode to be close to resonance with the excitonic transition. The detuning between the exciton and cavity energies is denoted as $\Delta = E_C(0) - E_X$ and is determined by the geometry of the cavity, in particular the cavity length L_C .

In addition, achieving the strong coupling regime requires the light-matter interaction to

overcome all dissipative processes in the system. This requires the use of high finesse and high Q-factor cavities, which can now be routinely produced.²⁶ For the sake of simplicity, we consider the case when the first cavity eigenmode is near the resonance with the excitonic transition. For this mode, the amplitude of the electric field is maximal at the center of the cavity and only the tubes located close to it efficiently participate in light-matter coupling. We thus consider a structure with few layers of densely packed parallel SWCNTs (see Fig. 1 (b)). High density arrays of carbon nanotubes can be fabricated nowadays using a spontaneous alignment technique,⁹ with minimal distance between the nanotubes up to 1 nm. However, in order to avoid the effects of the band structure modification due to electron hopping between adjacent tubes, in the current work we limit ourselves to the case of less dense ensembles where $l > 3$ nm, for which inter-tube electron hopping can be neglected. As we demonstrate below, ground state exciton brightening can be achieved even in this diluted regime.

Since the resonant wavelength of the cavity mode satisfies the condition $\lambda_C \gg nr$, where r is the distance between the layers of nanotubes and n is the number of layers, one can safely neglect the interaction modulation for a few layer system. To be specific, hereafter we choose $n = 10$. The interaction rate between the cavity eigenmode and the nanotube ensemble is defined as⁵²

$$g(k) = \sqrt{\frac{n}{l}} \sqrt{\frac{E_C(k)}{\varepsilon \varepsilon_0 L_C}} d_{cv} \psi_\alpha(x=0), \quad (4)$$

where $E_C(k) = E_C(0) + \hbar^2 k^2 / (2m_C)$ is the energy of the photonic mode written in the parabolic approximation, with $m_C = 2\pi\hbar\sqrt{\varepsilon}/(c\lambda_C)$ standing for the photon effective mass, $L_C = \lambda_C/2$ denoting the cavity length, and k being the in-plane wave vector. Here c denotes the speed of light, and ε is the dielectric permittivity of the media inside the cavity. The cavity is assumed to be filled by the polymer material PFO-BPy, with the structure effective permittivity $\varepsilon = 2.8$.³¹ We remind, however, that for the characterization of excitonic states we use the pure carbon dielectric constant $\varepsilon_C = 2$. Finally, the quantity $d_{cv} = 3ed/4$ denotes the interband transition dipole momentum (see Appendix for the details).

The properties of excitons in SWCNTs of different chiralities are presented in Table 1. It should be mentioned, that within a low-energy tight binding model, neglecting the trigonal warping effect,⁵³ the excitonic properties are defined solely by the diameter of nanotube. Thus, the identical parameters of nanotubes of (9,1) and (6,5) chirality are explained by the fact, that they have the same diameter, defined by $d = (a/\pi)\sqrt{n^2 + m^2 + nm}$, where $a = 2.46 \text{ \AA}$ is the graphene lattice constant, and n, m denote chiral indices.

Polariton modes arising from the exciton-photon coupling can be characterized using a conventional model of coupled oscillators with the Hamiltonian:²⁶

$$\hat{H} = \begin{pmatrix} E_C(k) & g(k)/2 \\ g(k)/2 & E_X \end{pmatrix}, \quad (5)$$

where for simplicity we have neglected the exciton dispersion because the effective mass of an exciton $m_X \gg m_C$. The eigenvalues of Hamiltonian (5) give the dispersions of the lower and upper polariton branches:

$$E_{\text{UP(LP)}} = \frac{E_X + E_C(k) \pm \Omega_R(k)}{2}, \quad (6)$$

with the Rabi splitting defined as

$$\Omega_R(k) = \sqrt{(E_X - E_C(k))^2 + g^2(k)}. \quad (7)$$

Results and Discussion. We can now proceed with the discussion of the properties of the emerging polariton modes, illustrated in Fig. 2 for the case of (10,0) nanotubes. For the chosen chirality the energy splitting between bright and dark excitons $\delta = E_X - E_X^{\text{dark}} = 29 \text{ meV}$.⁴⁰ It is clearly seen that the increase of tube concentration leads to the enhancement of the light-matter coupling, pulling down the energy of lower polariton branch. For maximal density, corresponding to the separation distance $l_{\text{min}} = 3 \text{ nm}$, the coupling strength is about $g \sim 55 \text{ meV}$. It is worth mentioning that both the square root dependence of the interaction

strength on the SWCNT density (see. Eq. (4) and coupling values are in good agreement with existing experimental results.³¹

As one can see from Fig. 2, for distances between the nanotubes close to $l_{min} = 3$ nm the energy of the polariton can reach the value of the energy of the dark exciton state. Introducing a non-zero detuning between excitonic and photonic modes, as shown in the lower panels of the figure, can pull the lower polariton state below the dark exciton state. At the same time, the excitonic fraction of the polariton state remains substantial, which means that the regime of the excitonic brightening is achievable. Fig.3 shows the position of the lower polariton energy versus the dark exciton energy and the excitonic fraction of the lower polariton as function of the distance between the nanotubes for various values of detuning, which demonstrates the aforementioned behavior.

We also examine the dependence of the coupling strength on the diameter of the SWCNT. We assume in each case that the cavity mode is tuned in resonance with the bright exciton energy and that the separation between the tubes is equal to 3 nm. In Fig. 4 the dependence of the coupling constant g is plotted versus the diameter of the tube. The dependence $g(d)$ demonstrates a universal $d^{-1/2}$ scaling. The latter dependence follows directly from Eq. (4), if one rewrites all the diameter-dependent quantities in their explicit form.

Finally, it should be noted that the ratio between the coupling strength and the exciton creation energy is strongly enhanced compared to the case of inorganic cavities and can reach the values $g/E_X \sim 0.1$. This means that the off-resonant light matter coupling terms can also play a non-negligible role in the considered geometry, and the regime of so-called ultra-strong coupling can be achieved.^{54,55} One should note as well that in principle even higher values of g can be reached if one decreases the distance between the nanotubes below l_{min} . In this case, however, the excitonic spectrum of the system can be substantially modified by hopping between neighboring tubes. Consideration of these effects goes beyond the scope of the present paper and is left for future investigation.

In conclusion, we have theoretically analyzed the regime of strong light-matter coupling

in a microcavity containing an ensemble of semiconducting carbon nanotubes. We have demonstrated that, for realistic parameters of the system, the value of the Rabi splitting can overcome the splitting between bright and dark energy states. As a result, a hybrid lower polariton mode can have an energy lower than that of the dark exciton, which results in brightening of the ground state of the system. This will lead to a drastic improvement of photoluminescence properties in nanotube-based systems. Finally, we note that graphene nanoribbons also have dark excitonic ground state.⁵⁶ The proposed here brightening scheme with similar values of the parameters should also work for ribbons due to equivalence of optical properties of both quasi-one-dimensional structures.^{57,58}

Appendix: Calculation of the dipole matrix element

In this section we present a derivation of the matrix elements of dipole transitions within the zone-folding tight-binding approximation. For graphene-based nanostructures it is convenient to deal with the matrix elements of the velocity operator, instead of the position matrix element, which allows one to express relevant physical quantities in terms of the graphene Fermi velocity v_F . These two approaches, however, are absolutely equivalent in the dipole approximation.⁵⁹ The two matrix elements are related by

$$\mathbf{v}_{nm} = \frac{i}{\hbar} \langle n | [H, \mathbf{r}] | m \rangle = i\omega_{nm} \mathbf{r}_{nm}, \quad (8)$$

where $\omega_{nm} = (E_n - E_m)/\hbar$ is the frequency of the transition.

To calculate velocity operator matrix elements for SWCNTs in the tight-binding model we employ the so-called gradient approximation (the term “effective mass approximation” is used in earlier literature).^{58,60–64} The optical selection rules resulting from such a calculation are in agreement with those in Refs.^{65–68} Using this approach, it is easy to show that the velocity matrix element dependence on the wave vector is not significant in semiconducting SWCNTs in the vicinity of the Dirac point, which corresponds to the conduction and valence

band edges. Therefore, the matrix element can be reasonably approximated by a constant value equal to the Fermi velocity of electrons in graphene v_F . Since we are interested in the transitions from the edges of the closest conduction and valence subbands, i.e., those that occur near the Dirac point, we can estimate the magnitude of the dipole moment operator matrix element as follows:

$$d_{cv} = e|r_{cv}| = \frac{ev_F\hbar}{E_g} = \frac{e\frac{\sqrt{3}at}{2\hbar}\hbar}{\frac{2at}{\sqrt{3}d}} = \frac{3ed}{4}, \quad (9)$$

where we have used Eqs. (8) and the fact that in the low-energy zone-folding approximation the energy gap is

$$E_g = 2\hbar v_F \Delta = 4\hbar v_F / (3d) = 2at / \sqrt{3}d, \quad (10)$$

where $v_F = \sqrt{3}at / (2\hbar)$ is the graphene Fermi velocity⁶⁹ in terms of the hopping intergral $t = 3.033 \text{ eV}^6$ and $\Delta = 2 / (3d)$ is the shift of the momentum quantization line from the Dirac point for any semiconducting SWCNT.^{53,70} For semiconducting $(n, 0)$ zigzag SWCNTs (n is not divisible by 3), $E_g = 2\pi t / (\sqrt{3}n)$.

Acknowledgements

The authors thank I. Chestnov, O. Kyriienko and C. A. Downing for valuable discussions. This work was supported by the EU FP7 ITN NOTEDEV (Grant No. FP7-607521) and EU H2020 RISE project CoExAN (Grant No. H2020-644076). V.Sh. and I.A.S. acknowledge support from mega-grant No. 14.Y26.31.0015 and goszadanie no 3.2614.2017/4.6 of the Ministry of Education and Science of the Russian Federation. V.A.S. and M.E.P. acknowledge support from FP7 IRSES projects CANTOR (Grant No. FP7-612285), and InterNoM (Grant No. FP7-612624). V.Sh. and V.A.S. thank the University of Iceland for hospitality during the work on this project.

References

- (1) Iijima, S. *Nature* **1991**, *354*, 56–58.
- (2) Charlier, J.-C.; Roche, S. *Rev. Mod. Phys.* **2007**, *79*, 677–732.
- (3) Park, S.; Vosguerichian, M.; Bao, Z. *Nanoscale* **2013**, *5*, 1727.
- (4) De Volder, M. F. L.; Tawfick, S. H.; Baughman, R. H.; Hart, A. J. *Science* **2013**, *339*, 535–539.
- (5) Sanchez-Valencia, J. R.; Dienel, T.; Gröning, O.; Shorubalko, I.; Mueller, A.; Jansen, M.; Amsharov, K.; Ruffieux, P.; Fasel, R. *Nature* **2014**, *512*, 61–64.
- (6) Saito, R.; Dresselhaus, G.; Dresselhaus, M. *Physical Properties of Carbon Nanotubes*; Imperial College Press: London, 1998; p 276.
- (7) Wei, X.; Tanaka, T.; Yomogida, Y.; Sato, N.; Saito, R.; Kataura, H. *Nat. Commun.* **2016**, *7*, 12899.
- (8) Titova, L. V.; Pint, C. L.; Zhang, Q.; Hauge, R. H.; Kono, J.; Hegmann, F. A. *Nano Lett.* **2015**, *15*, 3267–3272.
- (9) He, X.; Gao, W.; Xie, L.; Li, B.; Zhang, Q.; Lei, S.; Robinson, J. M.; Hároz, E. H.; Doorn, S. K.; Wang, W.; Vajtai, R.; Ajayan, P. M.; Adams, W. W.; Hauge, R. H.; Kono, J. *Nat. Nanotechnol.* **2016**, *11*, 633–638.
- (10) Shaver, J.; Kono, J. *Laser Photonics Rev.* **2007**, *1*, 260–274.
- (11) Spataru, C. D.; Ismail-Beigi, S.; Benedict, L. X.; Louie, S. G. *Phys. Rev. Lett.* **2004**, *92*, 077402.
- (12) Perebeinos, V.; Tersoff, J.; Avouris, P. *Phys. Rev. Lett.* **2004**, *92*, 257402.
- (13) Perebeinos, V.; Tersoff, J.; Avouris, P. *Nano Lett.* **2005**, *5*, 2495–2499.

- (14) Avouris, P.; Chen, Z.; Perebeinos, V. *Nat. Nanotechnol.* **2007**, *2*, 605–615.
- (15) Avouris, P.; Freitag, M.; Perebeinos, V. *Nat. Photonics(Review)* **2008**, *2*, 341–350.
- (16) Zaric, S.; Ostojic, G. N.; Shaver, J.; Kono, J.; Portugall, O.; Frings, P. H.; Rikken, G. L. J. A.; Furis, M.; Crooker, S. A.; Wei, X.; Moore, V. C.; Hauge, R. H.; Smalley, R. E. *Phys. Rev. Lett.* **2006**, *96*, 016406.
- (17) Ando, T. *J. Phys. Soc. Japan* **2006**, *75*, 024707.
- (18) Srivastava, A.; Htoon, H.; Klimov, V. I.; Kono, J. *Phys. Rev. Lett.* **2008**, *101*, 087402.
- (19) Kilina, S.; Ramirez, J.; Tretiak, S. *Nano Lett.* **2012**, *12*, 2306–2312.
- (20) Harutyunyan, H.; Gokus, T.; Green, A. A.; Hersam, M. C.; Allegrini, M.; Hartschuh, A. *Nano Lett.* **2009**, *9*, 2010–2014.
- (21) Shaver, J.; Kono, J.; Portugall, O.; Krstić, V.; Rikken, G. L. J. A.; Miyauchi, Y.; Maruyama, S.; Perebeinos, V. *Nano Lett.* **2007**, *7*, 1851–1855.
- (22) Zhou, W.; Nakamura, D.; Liu, H.; Kataura, H.; Takeyama, S. *Sci. Rep.* **2014**, *4*, 6999.
- (23) Xia, F.; Steiner, M.; Lin, Y.-M.; Avouris, P. *Nat. Nanotechnol.* **2008**, *3*, 609–613.
- (24) Legrand, D.; Roquelet, C.; Lanty, G.; Roussignol, P.; Lafosse, X.; Bouchoule, S.; Deleporte, E.; Voisin, C.; S., L. J. *Appl. Phys. Lett.* **2013**, *102*, 153102.
- (25) Miura, R.; Imamura, S.; Ohta, R.; Ishii, A.; Liu, X.; Shimada, T.; Iwamoto, S.; Arakawa, Y.; Kato, Y. *Nat. Comm.* **2014**, *5*, 5580.
- (26) Kavokin, A.; Baumberg, J.; Malpuech, G.; Laussy, F. *Microcavities*; Oxford University Press, New York: London, 2007.
- (27) Kna-Cohen, S.; Forrest, S. *Nat. Photonics* **2010**, *4*, 371–375.
- (28) Kna-Cohen, S.; Mayer, S.; Bradley, D. *Adv. Optical Mater.* **2013**, *1*, 827–833.

- (29) Daskalakis, K.; Maier, S.; Murray, R.; Kna-Cohen, S. *Nat. Materials* **2010**, *4*, 371–375.
- (30) Plumhof, J.; Stferle, T.; Mai, L.; Scherf, U.; Mahrt, R. *Nat. Materials* **2010**, *13*, 247–252.
- (31) Graf, A.; Tropf, L.; Zakharko, Y.; Zaumseil, J.; Gather, M. C. *Nat. Commun.* **2016**, *7*, 13078.
- (32) Zakharko, Y.; Graf, A.; Zaumseil, J. *Nano Lett.* **2016**, *16*, 6504–6510.
- (33) Graf, A.; Held, M.; Zakharko, Y.; Tropf, L.; Gather, M. C.; Zaumseil, J. *Nat. Mater.* **2017**, *16*, 911–918.
- (34) Ando, T. *J. Phys. Soc. Japan* **1997**, *66*, 1066–1073.
- (35) Kane, C. L.; Mele, E. J. *Phys. Rev. Lett.* **2003**, *90*, 207401.
- (36) Kane, C. L.; Mele, E. J. *Phys. Rev. Lett.* **2004**, *93*, 197402.
- (37) Uryu, S.; Ando, T. *Phys. Rev. B* **2006**, *74*, 155411.
- (38) Ando, T.; Uryu, S. *Phys. Status Solidi* **2009**, *6*, 173–180.
- (39) Chang, E.; Bussi, G.; Ruini, A.; Molinari, E. *Phys. Rev. Lett.* **2004**, *92*, 196401.
- (40) Spataru, C. D.; Ismail-Beigi, S.; Capaz, R. B.; Louie, S. G. *Phys. Rev. Lett.* **2005**, *95*, 1–4.
- (41) Jiang, J.; Saito, R.; Samsonidze, G. G.; Jorio, A.; Chou, S. G.; Dresselhaus, G.; Dresselhaus, M. S. *Phys. Rev. B* **2007**, *75*, 035407.
- (42) Zhao, H.; Mazumdar, S. *Phys. Rev. Lett.* **2004**, *93*, 157402.
- (43) Pedersen, T. *Phys. Rev. B* **2003**, *67*, 2–5.
- (44) Maultzsch, J.; Pomraenke, R.; Reich, S.; Chang, E.; Prezzi, D.; Ruini, A.; Molinari, E.; Strano, M. S.; Thomsen, C.; Lienau, C. *Phys. Rev. B* **2005**, *72*, 241402.

- (45) Hartmann, R. R.; Shelykh, I. A.; Portnoi, M. E. *Phys. Rev. B* **2011**, *84*, 035437.
- (46) Downing, C. A.; Portnoi, M. E. *Phys. Rev. A* **2014**, *90*, 052116.
- (47) Loudon, R. *Am. J. Phys.* **1959**, *27*, 649.
- (48) Wang, F.; Dukovic, G.; Brus, L. E.; Heinz, T. F. *Science* **2005**, *308*, 838–841.
- (49) Bányai, L.; Galbraith, I.; Ell, C.; Haug, H. *Phys. Rev. B* **1987**, *36*, 6099–6104.
- (50) Ogawa, T.; Takagahara, T. *Phys. Rev. B* **1991**, *43*, 14325–14328.
- (51) Ogawa, T.; Takagahara, T. *Phys. Rev. B* **1991**, *44*, 8138–8156.
- (52) Burstein, E.; Weisbuch, C. *Confined Electrons and Photons: New Physics and Applications*; Springer Science+Business Media: New York, 1995; p 67.
- (53) Saito, R.; Dresselhaus, G.; Dresselhaus, M. *Phys. Rev. B* **2000**, *61*, 2981–2990.
- (54) Ciuti, C.; Bastard, G.; Carusotto, I. *Phys. Rev. B* **2005**, *72*, 115303.
- (55) de Liberato, S. *Phys. Rev. Lett.* **2014**, *112*, 016401.
- (56) Yang, L.; Cohen, M. L.; Louie, S. G. *Nano Lett.* **2007**, *7*, 3112–5.
- (57) Portnoi, M. E.; Saroka, V. A.; Hartmann, R. R.; Kibis, O. V. Terahertz Applications of Carbon Nanotubes and Graphene Nanoribbons. 2015 IEEE Comput. Soc. Annu. Symp. VLSI. 2015; pp 456–459.
- (58) Saroka, V. A.; Shuba, M. V.; Portnoi, M. E. *Phys. Rev. B* **2017**, *95*, 155438.
- (59) Berestetskii, V. B.; Lifshitz, E. M.; Pitaevskii, L. P. *Quantum Electrodynamics*; Butterworth-Heinemann: Oxford, 1997.
- (60) Wannier, G. H. *Rev. Mod. Phys.* **1962**, *34*, 645–655.

- (61) Blount, E. In *Solid State Phys.*; Seitz, F., Turnbull, D., Eds.; Academic Press: New York, 1962; Vol. 13; pp 305–373.
- (62) Dresselhaus, G.; Dresselhaus, M. S. *Phys. Rev.* **1967**, *160*, 649–679.
- (63) Lew Yan Voon, L. C.; Ram-Mohan, L. R. *Phys. Rev. B* **1993**, *47*, 15500–15508.
- (64) Lin, M. F.; Shung, K. W. K. *Phys. Rev. B* **1994**, *50*, 17744–17747.
- (65) Ajiki, H.; Ando, T. *Phys. B Condens. Matter* **1994**, *201*, 349–352.
- (66) Milošević, I.; Vuković, T.; Dmitrović, S.; Damnjanović, M. *Phys. Rev. B* **2003**, *67*, 165418.
- (67) Jiang, J.; Saito, R.; Grüneis, A.; Dresselhaus, G.; Dresselhaus, M. *Carbon N. Y.* **2004**, *42*, 3169–3176.
- (68) Malić, E.; Hirtschulz, M.; Milde, F.; Knorr, A.; Reich, S. *Phys. Rev. B* **2006**, *74*, 195431.
- (69) Castro Neto, A. H.; Guinea, F.; Peres, N. M. R.; Novoselov, K. S.; Geim, A. K. *Rev. Mod. Phys.* **2009**, *81*, 109–162.
- (70) Samsonidze, G. G.; Saito, R.; Jorio, A.; Pimenta, M. A.; Souza Filho, A. G.; Grüneis, A.; Dresselhaus, G.; Dresselhaus, M. S. *J. Nanosci. Nanotechnol.* **2003**, *3*, 431–458.

Graphical TOC Entry

